PHYSICAL REVIEW B **95**, 245403 (2017)

Finite-temperature phase diagram and critical point of the Aubry pinned-sliding transition in a two-dimensional monolayer

Davide Mandelli,[1,2] Andrea Vanossi,[1,3] Nicola Manini,[1,3,4] and Erio Tosatti[1,3,5]
[1]*International School for Advanced Studies (SISSA), Via Bonomea 265, 34136 Trieste, Italy*
[2]*Tel Aviv University, Tel Aviv 6997801, Israel*
[3]*CNR-IOM Democritos National Simulation Center, Via Bonomea 265, 34136 Trieste, Italy*
[4]*Dipartimento di Fisica, Università degli Studi di Milano, Via Celoria 16, 20133 Milano, Italy*
[5]*International Centre for Theoretical Physics (ICTP), Strada Costiera 11, 34014 Trieste, Italy*
(Received 14 April 2017; published 6 June 2017)

The Aubry unpinned-pinned transition in the sliding of two incommensurate lattices occurs for increasing mutual interaction strength in one dimension and is of second order at $T = 0$, turning into a crossover at nonzero temperatures. Yet, real incommensurate lattices come into contact in two dimensions, at finite temperature, generally developing a mutual Novaco-McTague misalignment, conditions in which the existence of a sharp transition is not clear. Using a model inspired by colloid monolayers in an optical lattice as a test two-dimensional (2D) case, simulations show a sharp Aubry transition between an unpinned and a pinned phase as a function of corrugation. Unlike one dimension, the 2D transition is now of first order, and, importantly, remains well defined at $T > 0$. It is heavily structural, with a local rotation of moiré pattern domains from the nonzero initial Novaco-McTague equilibrium angle to nearly zero. In the temperature (T)-corrugation strength plane, the thermodynamical coexistence line between the unpinned and the pinned phases is strongly oblique, showing that the former has the largest entropy. This first-order Aubry line terminates with a novel critical point $T = T_c$, marked by a susceptibility peak. The expected static sliding friction upswing between the unpinned and the pinned phase decreases and disappears upon heating from $T = 0$ to $T = T_c$. The experimental pursuit of this novel scenario is proposed.

DOI: 10.1103/PhysRevB.95.245403

I. INTRODUCTION

There is in tribology—the science of friction and adhesion—a longstanding interest in models of periodic solid interfaces that are incommensurate, where the crystal unit cells facing each other are fundamentally mismatched in either size or angle or both, so that they cannot fit in a common unit cell of any finite size. While in the macroscopic world it is generally difficult to realize a perfectly incommensurate interface because of defects, irregularities, and temperature, in nanotribology [1,2] there are well-defined nanoscale realizations of incommensurate crystal interfaces, such as graphene and other two-dimensional (2D) sheets [3,4], rare-gas monolayers [5], and colloid monolayers in an optical lattice [6,7]. The present work is devoted to understanding the relative state of pinning of an idealized, yet well-defined realization of this type of 2D contact, focusing especially on its evolution under conditions of finite temperature, a question totally unexplored so far.

We begin with a brief review, which starts from the 1D Frenkel-Kontorova (FK) model [8,9], consisting of a harmonic chain of classical point particles in a static sinusoidal potential of amplitude W_0, which acts as a corrugation opposing chain sliding. Incommensurability between the mean interparticle spacing a_c and the sinusoidal potential wavelength a_p occurs when the ratio $\rho = a_c/a_p$ is irrational. With respect to the unperturbed chain, the incommensurate potential causes a distortion of the particle positions that can be described by a deformation of the chain's local phase $\Phi(x)$ relative to the reference phase of the corrugation sinusoid. As the chain-sinusoid interaction increases from the noninteracting straight behavior $\Phi_0(x) = (\rho - 1)x$ at $W_0 = 0$, the phase deforms into a smooth staircase shape with the same mean slope $(\rho - 1)$, but now sporting nearly commensurate and horizontal steps where $\Phi(x)$ is approximately constant, separated by jumps, called solitons or misfit dislocations, or kinks, and antisolitons (antikinks), where most of the misfit stress associated with $\nabla\Phi$ is concentrated. Incommensurability implies that the total energy E of the chain is in all cases strictly independent of its center-of-mass position, $\delta E/\delta\Phi = 0$. Because of this, it had long been held that the translational dynamics of an incommensurate interface should always be gapless—causing in this case the chain state to be unpinned and thus shiftable by an arbitrarily small force. In the 1980s Aubry proved mathematically that this is not always so. The 1D incommensurate FK model displays at $T = 0$ and for fixed harmonic spring constant a sharp phase transition [10] between an unpinned phase where the corrugation is weak [soliton widths larger then or comparable to that of the steps, small overall distortion $\Phi(x) - (\rho - 1)x$], and a pinned phase, realized above a critical corrugation magnitude W_{0c}, where the distortion is large, solitons are narrow, and the phase distortion is large. Above W_{0c}, whose magnitude depends on precise parameters and on incommensurability, the chain develops a nonzero gap against sliding.

The well-known physical essence of the Aubry transition is that the relative probability to find a particle exactly at a potential maximum—probability that is finite so long as the chain is unpinned—drops mathematically to zero at $W_0 > W_{0c}$, constituting a self-generated constraint to the chain center-of-mass dynamics and to its sliding motion at $T = 0$ [11]. That is, despite $\delta E/\delta\Phi = 0$, the dynamical constraint limits phase-space accessibility, effectively breaking ergodicity and causing the onset of static friction, pinning of the chain against

free sliding under an infinitesimally small external force. Even if it is, for any finite system size and within mean field, a regular structural and thermodynamic transition [12], the Aubry transition does not possess a proper Landau-type order parameter. It has instructively been characterized by a disorder parameter measuring the extension of the forbidden phase space, a concept which we will make use of later. Even if the step-terrace deformation of the chain's phase $\Phi(x)$ retains a qualitatively similar nature to that in the unpinned state, the solitons evolve from broad and overlapping to nonoverlapping and atomically sharp, and both static and dynamic friction change at the transition. In the unpinned phase, the chain slides under any applied force however weak, leading to a state of flow of the solitons. This absence of static friction is sometimes referred to as superlubricity or structural lubricity in the friction community. In the pinned state, chain sliding requires a static friction threshold force to be overcome, before sliding sets in.

The $D = 1$, $T = 0$ physics being well understood, it does remain rather academic unless it can be brought closer to the real, in our case nanotribological, world [13–16]. Real incommensurate lattices come into contact at an interface, which is $D = 2$ dimensional. Moreover, temperature is always finite and often large. Although the physics of the unpinned-pinned transition [9] is usually and reasonably assumed to be the same in $D = 2$ and $T > 0$ as that of Aubry's case in $D = 1$ and $T = 0$ that assumption is neither theoretically proven nor at least demonstrated in a specific experimentally relevant example. Clearly, the two regimes of essential unpinning and of strong pinning must surely exist for flat 2D incommensurate contacts. However, whether there is or is not between them a sharp transition as a function of the contact strength, and if so precisely what kind of transition, must still be determined. At $T = 0$, moreover, the 1D Aubry transition is continuous and critical as a function of mechanical parameters. Although in mean-field theory the second-order Aubry transition may extend to finite temperature [12], in reality in one dimension the sharp phase transition is strictly limited to $T = 0$, turning into a smooth crossover at any finite temperature [9].

A recent study [17] of a 2D model colloid monolayer in an incommensurate optical lattice provides the first interesting example of such a transition in a real class of systems where experiments are actively going on [6,18]. That study revealed at $T = 0$ a 2D Aubry-type unpinned-pinned transition, which is, unlike the 1D case, of first order for increasing corrugation. In that transition the Novaco-McTague misalignment angle [19], a specific 2D feature, plays an important role. Moreover, the two components of the total (potential) energy, namely the interparticle and the particle-substrate-potential terms, undergo opposite and compensating jumps. The evolution of this 2D unpinning-pinning transition in the real finite-temperature situation remains as yet unknown.

Here we show, exploiting the same 2D colloid monolayer/optical lattice model as a relevant system, which we can study by molecular dynamics (MD) simulations, that the Aubry-like transition remains well defined and of first order at nonzero temperature, where it gives rise to a clear phase line between the unpinned and the pinned states. The large positive slope of this line indicates via Clausius-Clapeyron's equation that the unpinned phase has the largest entropy, revealing some collapse of accessible phase space in the pinned phase. A disorder parameter, the 2D version of Coppersmith-Fisher's 1D one [11], is correspondingly identified, and its jump is demonstrated at the onset of pinning. From the geometric viewpoint, the 2D Aubry transition in this model system is heavily structural. Its main feature is a rotation of local moiré pattern domains from the nonzero Novaco-McTague-like misalignment angle in the weak-corrugation unpinned phase to nearly zero in the strong-corrugation pinned phase. The two phases appear to possess the same spatial symmetry. Thus the first-order line is accordingly expected and actually found to terminate at a high-temperature critical point, where unpinned and pinned characters are lost and therefore merge. Limitations of simulation size and time do not permit here a characterization of this critical point, which qualitative considerations would tentatively place in the universality class of the gas-liquid transition. As in liquid gas, the particle-particle energy and the entropy jumps contributing to the free energy are equal in magnitude at the transition; however, in this Aubry case they have the same sign rather than opposite signs, their positive sum exactly compensating the gain of periodic potential energy (a term absent in liquid gas).

After this characterization of equilibrium properties, we address tribological and dynamical questions by carrying out further simulations and extracting static friction under an external force. The change from zero to finite static friction characterizes the unpinned and pinned nature, respectively, confirming a change from lubricity of the unpinned phase to sticking of the pinned phase, which persists at $T > 0$, and only vanishes at the terminal critical temperature.

II. MODEL AND SIMULATIONS

Following our previous $T = 0$ work [7,17] we describe the colloidal particles as classical point objects interacting via a screened repulsive Coulomb potential

$$V(r) = \frac{Q}{r}\exp(-r/\lambda_{\mathrm{D}}), \tag{1}$$

where r is the interparticle distance, Q is the coupling strength, and λ_{D} is a Debye screening length. Particle motion is restricted to two dimensions, where unperturbed colloids form a triangular lattice of spacing a_c in the (x,y) plane. The externally added 2D periodic triangular corrugation potential

$$\begin{aligned} W(\mathbf{r}) &= -W_0\frac{2}{9}\left[\frac{3}{2} + 2\cos\frac{2\pi x}{a_l}\cos\frac{2\pi y}{\sqrt{3}a_l} + \cos\frac{4\pi y}{\sqrt{3}a_l}\right] \\ &= W_0 w(\mathbf{r}) \end{aligned} \tag{2}$$

has strength W_0 and periodicity a_l, representing the experimental optical lattice. Here we restrict particle motion to two dimensions, even if real colloids can move in three dimensions, because we are interested in the 2D problem in the first place. Moreover, the experimental setup [6] implements an additional strong confining laser force in the z direction, which suppresses drastically all vertical fluctuations to less than 5% of the

particle diameter. The total potential energy of N_p particles is

$$H = \sum_{i=1}^{N_p} \left[W(\mathbf{r}_i) + \frac{1}{2} \sum_i \sum_{j \neq i} V(r_{ij}) \right]. \quad (3)$$

The jth particle displacement $\mathbf{r}_j$ obeys the Langevin equation

$$m\ddot{\mathbf{r}}_j + \eta \dot{\mathbf{r}}_j = -\nabla_{\mathbf{r}_j} \left[\sum_{i \neq j} V(r_{ij}) + W(\mathbf{r}_j) \right] + \xi R(t), \quad (4)$$

where η is the viscosity of the solvent, and $R(t)$ is a δ-correlated stationary Gaussian process, satisfying

$$\langle R(t) \rangle = 0 \quad (5)$$

$$\langle R(t) R(t') \rangle = \delta(t - t'). \quad (6)$$

The fluctuation-dissipation theorem is satisfied by setting $\xi = \sqrt{2\eta k_B T}$, where k_B is Boltzmann's constant and T is the temperature. An overdamped dynamics of these particles is generated by integrating the equations of motion with a large viscous coefficient $\eta = 28$ and $Q = 10^{13}$, $\lambda_D = 0.03$. In our simulations we further assume 2D periodic boundary conditions (PBCs). Results are expressed in terms of the same system of units defined in Table I of Ref. [17]. In these units, very roughly inspired by experimental systems [6], $T \sim 0.04$ corresponds to room temperature.

Incommensurability between the particle monolayer and the 2D periodic potential generally arises both from their different lattice spacing and from their relative misalignment (rotation) angle. Any chosen misalignment angle between the corrugation $W(\mathbf{r})$ and the colloidal lattice can be implemented by means of a suitably chosen supercell, as follows [20]. The two lattices are defined by the pairs of primitive vectors $\mathbf{a}_1 = a_l(1,0)$, $\mathbf{a}_2 = a_l(0.5, \sqrt{3})$, and $\mathbf{b}_1 = a_c(\cos\theta, \sin\theta)$, $\mathbf{b}_2 = a_c[\cos(\theta + \pi/3), \sin(\theta + \pi/3)]$. An arbitrary supercell-periodic structure, meant to approximate the real incommensurate system, is realized when four integers are found that satisfy the matching condition $n_1\mathbf{a}_1 + n_2\mathbf{a}_2 = m_1\mathbf{b}_1 + m_2\mathbf{b}_2$. The supercell is a larger triangular lattice of size $L = |m_1\mathbf{b}_1 + m_2\mathbf{b}_2|$, containing a total number of particles $N_p = m_1^2 + m_1 m_2 + m_2^2$. We fix $a_c = 1$ and vary $n_{1,2}$, $m_{1,2}$ in search of structures with a mismatch $\rho = a_l/a_c \approx 3/(1 + \sqrt{5}) \simeq 0.927$—close to the experimental values of Ref. [6]—and θ near the desired value, with the obvious additional constraint that the number of particles N_p should not be too large. We consider in practice the aligned configuration $\theta = 0$, plus misaligned configurations: $\theta \simeq 5^\circ$, $\theta \simeq 10^\circ$, and $\theta_{opt} \simeq 2.54^\circ$. The latter is close to the (Novaco-McTague) equilibrium misalignment angle $\theta_{NM} \simeq 2.58^\circ$ predicted by weak-coupling elastic theory for the present parameters and $\rho = 0.927$ [19,21]. We could have equally chosen to study an overdense case, $\rho > 1$. However, the underdense regime $\rho < 1$, which we have chosen is better suited because overdense local compressions may favor large bucklings of particles out of the plane, and because the energetics (not symmetrical with respect to $\rho > 1$) is less convenient in that case. The supercell parameters adopted here are the same as in Ref. [17].

The mismatch between the 2D particle lattice and the periodic potential produces a moiré pattern corresponding to a superlattice of hexagonal domains where particles and potential are mutually nearly commensurate, separated by a honeycomb network of (anti)soliton lines whose thickness decreases with increasing corrugation strength. Examples of the moiré superstructures are shown in Fig. 1. We recall here for clarity the relation [22] between the misalignment angle θ and the moiré orientation α

$$\cos\theta = \rho^{-1} \sin^2\alpha + \cos\alpha \sqrt{1 - \rho^{-2}\sin^2\alpha}\,. \quad (7)$$

The moiré pattern visually underlines the difference between particles whose position is near the energetically favorable potential minima, and others near the unfavorable potential maxima. In the 1D case studied in the 1980s, the presence or absence of pinning was described by a disorder parameter Ψ, roughly measuring the radius of the neighborhood of each potential maximum, which, at $T = 0$, turned from (partly) occupied in the unpinned state to exactly empty in the pinned state [11]. The (tribological) essence of the Aubry transition is that when all states are accessible and the disorder parameter is zero, the incommensurate system is unpinned and can slide under an arbitrarily small force, whereas when the occupancy of potential maxima and their neighborhood drops to zero and therefore the disorder parameter is nonzero, the system is pinned and free sliding is impeded. Looking for a 2D analog of the disorder parameter we measure [17] the fraction $\Psi = N_s/N_p$ of particles that populate the geometrically defined, bow-tie-shaped area where the periodic potential $W(x,y)$ is repulsive, exceeding its saddle-point value (see Fig. 2). The value of $\Psi(T, W_0)$ and especially its jump will be used to characterize phase boundaries in the (W_0, T) plane phase diagram.

The phase transition is studied as follows. At each fixed and nonzero value of T we carry out two series of simulations, the

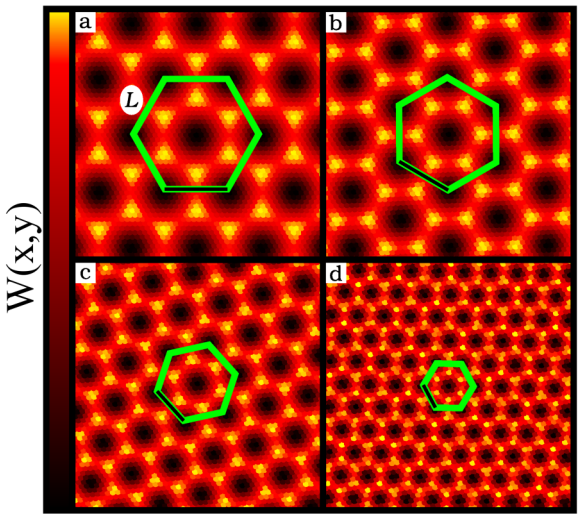

FIG. 1. Examples of the moiré patterns obtained at $\rho \simeq 0.927$ for misfit angles (a) $\theta = 0$, (b) $\theta_{opt} \simeq 2.54^\circ$, (c) $\theta \simeq 5^\circ$, and (d) $\theta \simeq 10^\circ$. Each dot represents a particle, whose color reflects the local corrugation potential $W(x,y)$: dark for potential minima, bright for maxima. A small portion of the simulation supercells is displayed, containing an undistorted monolayer, at $W_0 = 0$. According to Eq. (7), at $\theta_{opt} \simeq 2.54^\circ$, (b), the moiré orientation is $\alpha \simeq 30^\circ$. As θ increases beyond θ_{opt}, the superstructure periodicity L shrinks rapidly and rotates all the way to $\alpha \simeq 60^\circ$ (d).

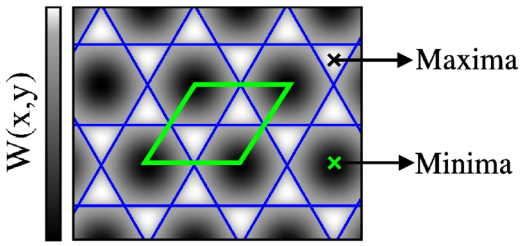

FIG. 2. Color map of the 2D periodic triangular substrate potential $W(x,y)$. A primitive cell is highlighted at the center. Isolines are drawn corresponding to the saddle-point value separating adjacent minima.

first starting from an unpinned configuration at an adequately small value of W_0, which is then increased in small steps ΔW_0, the second starting from a pinned configuration at an adequately large value of W_0, which is then decreased in a similar fashion. We generally adopt $\Delta W_0 = 0.005$–0.01, reducing it to $\Delta W_0 = 0.001$ in the parameter region straddling the transition. For each value of W_0 the MD simulation time is chosen so as to ensure thermal equilibrium. Each run at $W_0 \pm \Delta W_0$ is started from a configuration equilibrated at the previous step in the sequence. Thermal equilibration is checked by monitoring the disorder parameter Ψ, which generally increases or decreases with simulation time, eventually reaching a plateau. We could in principle have used the convergence of another mechanically defined variable, such as the internal energy, to monitor equilibration. However, internal energy fluctuations, related to specific heat, are harder to handle than those of the disorder parameter, which turns out to be a better choice in practice. All relevant observables are computed from time averages along the trajectories, discarding the initial transient time.

All equilibrium simulations described here are carried out with 2D PBCs, corresponding to NVT canonical ensemble (as opposed to a NPT ensemble, here inaccessible). On account of the constant volume (in this case, constant area), a first-order phase transition in general implies an intermediate two-phase coexistence region, since the unpinned and pinned phases generally differ in pressure as well as in disorder parameter. The existence of two separate phase boundaries in the (W_0,T) plane is indeed signaled by two different possible stable values of the disorder parameter Ψ—in practice by two noncoincident upward and downward jumps of Ψ for increasing or decreasing potential strength W_0. As it turns out for our working parameters the width $W_2 - W_1$ of the two-phase region is narrow. Its midpoint line $W_0^* = (W_1 + W_2)/2$ (where W_1 and W_2 are the border values) is therefore adequately representative of an underlying effective constant-pressure first-order phase line. In this way we avoid the complex questions that would otherwise arise in order to extract a constant-pressure result, a volume change being difficult to combine with the (rigid) periodic potential and the requirement of fixed incommensurability.

The global angular orientation of the monolayer relative to the lattice potential is held fixed by the PBCs, independently of temperature. While that is an assumption reflecting a computational necessity, it does represent those experimental realizations where very large, practically infinite colloid islands are not expected to execute global rotations. Actually, temperature, besides smearing somewhat the periodic potential, would nudge the overall equilibrium orientation angle in the direction where the total-energy growth is softer. However, calculations at $T = 0$ showed [17,21] that the angle of minimum energy (2.54° in our case) is rather independent on the potential magnitude, as also suggested by weak-coupling theory [19], making the optimal orientation angle insensitive to thermal smearing. Moreover, the $T = 0$ total energy is rather symmetric around the minimum, equally soft on both sides, so that no orientational nudging is expected. It is therefore very reasonable to adopt the same optimal $T = 0$ global orientation angle independent of temperature.

The Helmholtz free-energy of the monolayer is $F = U + W - TS$, where $U = \frac{1}{2}\langle \sum_i \sum_{j\neq i} V(r_{ij})\rangle$, $W = \langle \sum_i W(\mathbf{r}_i)\rangle$, and S is the entropy. By crossing the first-order transition upon variable W_0 and constant T,

$$\Delta U + \Delta W - T\Delta S = \Delta F = 0\,. \tag{8}$$

Simulations yield directly ΔU and ΔW, both of them mechanical quantities, across the transition. Through Eq. (8) we obtain the entropy jump ΔS at the unpinning-pinning transition. Of course, since no thermodynamic results such as ΔS are correctly represented at low temperatures by a totally classical simulation, it must be understood that all results are valid only from some (small) finite temperature upward. In future comparisons with experimental data this will not be a problem, because colloidal experiments are carried out at room temperature.

Finally, the static friction force F_s of the monolayer, which actually determines the presence or absence of pinning, is obtained by applying a driving force F_d to each colloid, generally along a high-symmetry direction of the laser substrate potential. Briefly, the external force is increased in steps ΔF, and for each value of the force a simulation is carried out where the duration is fixed in such a way that a single free particle would move by a distance of $\Delta x = 5.5a_l$. The monolayer is considered to be sliding (i.e., depinned) if the total displacement of its center-of-mass at the end of the simulation is $\Delta x_{\rm com} > 2.0a_l$.

III. RESULTS: FINITE TEMPERATURE 2D AUBRY TRANSITION AND PHASE DIAGRAM

The simulation protocol just outlined yields direct evidence that the first-order phase transition between an unpinned phase at small corrugation magnitude W_0 and a pinned phase at large W_0 persists at finite temperature. All thermodynamic quantities (except, at constant pressure, the total Gibbs free energy) jump at the transition, as shown in Fig. 3. Figure 4 shows the phase diagram, where the two-phase coexistence region (at constant volume) is very narrow, indicating that constant volume and constant pressure are very similar. Thus Gibbs and Helmholtz free energies only differ by a constant, and the jumps ΔU, ΔW approximately coincide. While at $T = 0$ $\Delta U = -\Delta W$ are opposite and compensate exactly, at finite temperature entropy kicks in, and near T_c the approximate equality $-T\Delta S + \Delta U = \Delta W$ holds. The large negative jump ΔW at pinning indicates that in the pinned state particles

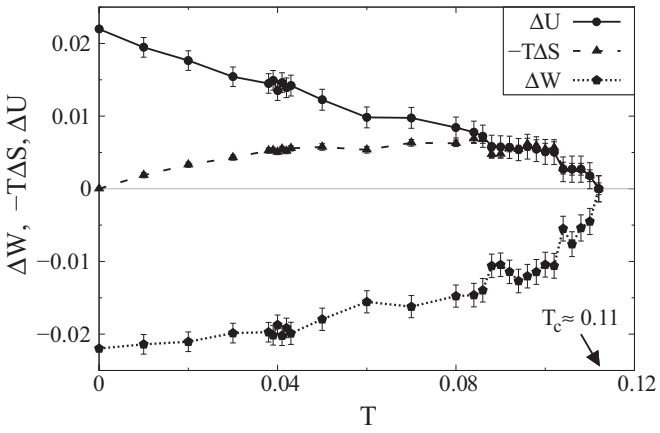

FIG. 3. The temperature dependence of the three contributions to the free energy per particle evaluated across the coexistence line. ΔW, $-T\Delta S$, ΔU correspond, respectively, to the change in substrate potential energy, entropy, and interparticle energy between the pinned and the unpinned phase.

benefit much more from the external potential minima. That gain is compensated by a corresponding worsening of particle-particle interactions and of entropy, both much better in the unpinned phase. Besides these reasonable outcomes, we observe in addition that at least close to T_c, $-T\Delta S \sim \Delta U$, an unexpected approximate equality for which we found no good explanation.

The phase diagram of Fig. 4 also shows that the unpinned-pinned transition is heavily right leaning with temperature, ending at $W_{0c} \simeq 0.44$, $T_c \simeq 0.11$, the latter to be compared with $T = 0.04$, the model room temperature). The unpinned phase therefore possesses a much larger entropy than the pinned phase. Moreover, the inverse slope $d(W_0^*/W_{0c})/d(T/T_c) = 0.50 \pm 0.05$ is quite small, in contrast with liquid-gas slopes $d(P/P_c)/d(T/T_c) \simeq 3, 4, 6.5$ for H_2O, a van der Waals fluid [23], and Ar [24], respectively.

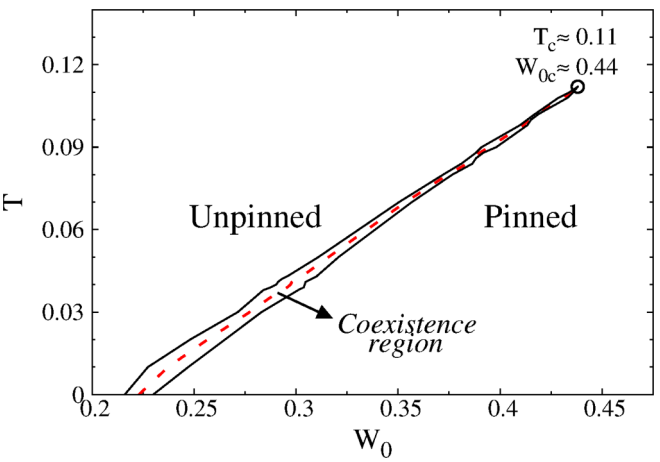

FIG. 4. Phase diagram in the (W_0, T) plane defined by the substrate corrugation strength and temperature. At each T the region of phase coexistence is confined to a very narrow interval (W_1, W_2) of corrugations, as shown by the continuous lines in the plot. The dashed curve shows the average value $W_0^* = (W_1 + W_2)/2$, which has been used to define the coexistence line adopted in our thermodynamic analysis of the transition. The steady slope of the coexistence line indicates that the unpinned phase retains consistently a higher entropy than the pinned phase.

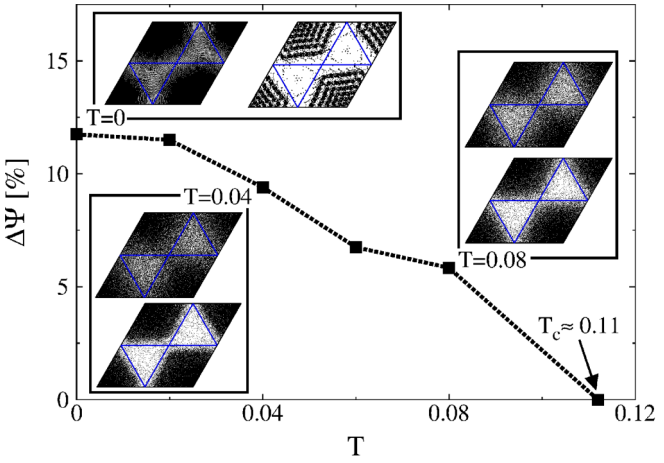

FIG. 5. The jump $\Delta\Psi$ of the 2D disorder parameter across the first-order phase transition is reported as a function of temperature. For a few values of T, the insets illustrate the corresponding change in the population of the regions above the saddle-point value. There the positions of all particles are reported folded inside one primitive cell of the substrate potential (at finite T several snapshots along the trajectory have been considered). Table I reports the two corrugation amplitudes $W_{1,2}$ used for the insets and for the definition of $\Delta\Psi$. At the critical temperature $T_c \simeq 0.11$ the transition becomes of second order and Ψ varies smoothly across it: here we just set $\Delta\Psi(T_c) = 0$ for simplicity.

Finally, Fig. 5 summarizes our resulting disorder parameter for the Aubry-type transition of the 2D colloid model at $\rho = 0.927$ as a function of temperature. Similar to the 1D case [11], the transition is characterized by a sudden drop of the number of particles lying near the maxima of $W(x, y)$. This is demonstrated by the jump $\Delta\Psi$ of the 2D disorder parameter, which is finite up to $T = T_c \simeq 0.11$, where it disappears.

IV. STRUCTURAL: LOCAL COMMENSURATE ROTATION

The drastic energy changes taking place across the transition have a clear structural origin. As was the case at $T = 0$, the moiré pattern conserves its shape and symmetry across the unpinned-pinned transition, but the central domains enclosed

TABLE I. The values of the substrate potential strength W_0 used to define the jump $\Delta\Psi$ of the disorder parameter at the transition, for the temperatures T shown in Fig. 5. Values of W_1 (W_2) have been taken in the unpinned (pinned) phase immediately before (after) the coexistence region in the (W_0, T) plane.

T	W_1	W_2
0	0.216	0.230
0.02	0.247	0.270
0.04	0.288	0.306
0.06	0.331	0.229
0.08	0.371	0.382

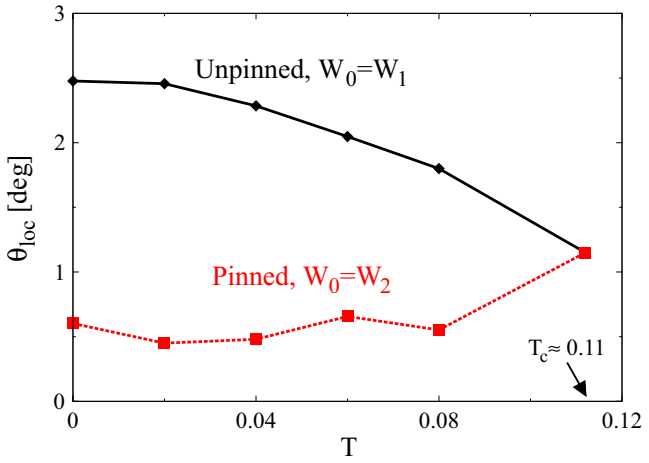

FIG. 6. The local angular orientation of the colloidal monolayer defined in Eq. (9) as a function of temperature. The black continuous curve shows the orientation measured at $W_0 = W_1$ in the unpinned phase, while the red dashed curve is the corresponding local alignment in the pinned phase at $W_0 = W_2$. Temperatures T and corrugations $W_{1,2}$ considered here are the same as those of Fig. 5, also reported in Table I. At $T = T_c \simeq 0.11$ there is no discrete jump in the local orientation: the point reported in the plot has been measured at a single value $W_0 = 0.439$, at the middle of the continuous crossover.

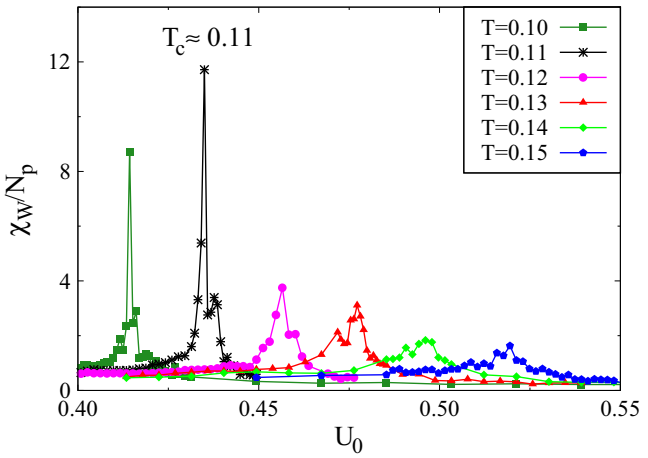

FIG. 7. The susceptibility χ_W defined in Eq. (10) as a function of the substrate corrugation for different temperatures. A sharp peak appears when approaching $T_c \simeq 0.11$, confirming the presence of a critical point.

by the honeycomb-shaped network of domain walls undergo a sharp structural transformation [17]. At pinning, the portion of 2D lattice inside each hexagon rotates transforming from misaligned and incommensurate to approximately aligned and commensurate with the underlying periodic potential. This transformation can be followed by calculating the average local lattice orientation of the colloidal monolayer defined as

$$\theta_{\rm loc} = \left\langle \frac{1}{M} \sum_{\langle i,j \rangle} \mathrm{mod}\left(\theta_{ij}, \frac{\pi}{3}\right) \right\rangle, \tag{9}$$

where the sum is over all M pairs $\langle i,j \rangle$ of nearest-neighbor particles with coordination six (excluding therefore the soliton regions), and θ_{ij} is the angle between the relative position vector $\mathbf{r}_i - \mathbf{r}_j$ and the x axis. Figure 6 reports $\theta_{\rm loc}$ as a function of temperature for both the pinned and unpinned phases. It is clear that below $T = T_c \simeq 0.11$, and as the corrugation increases across the transition, all local hexagonal domains between solitons locally rotate away from the initial Novaco-McTague orientation and back in approximate registry with the substrate. The sharp drop of particle-potential energy W that was seen to take place at pinning corresponds precisely to the falling of most particles inside each hexagonal cell into potential minima, an event that occurs at local commensurability.

V. UNPINNED-PINNED CRITICAL POINT

Results of Figs. 5 and 6 show that first-order discontinuities connected with the unpinned-pinned transition diminish with increasing temperature, until they vanish near $T = T_c \simeq 0.11$, at $W_0 = W_{0c} \simeq 0.44$. These parameters appear to identify a novel 2D critical point. In order to ascertain criticality we study the susceptibility

$$\chi_W = -\frac{\partial \left\langle \sum_i w(\mathbf{r}_i) \right\rangle}{\partial W_0} = \frac{\left\langle [\sum_i w(\mathbf{r}_i)]^2 \right\rangle - \left\langle \sum_i w(\mathbf{r}_i) \right\rangle^2}{k_B T}, \tag{10}$$

which is obtained from the thermal fluctuations of the dimensionless triangular substrate potential $W/W_0 = \langle \sum_i w(\mathbf{r}_i) \rangle$.

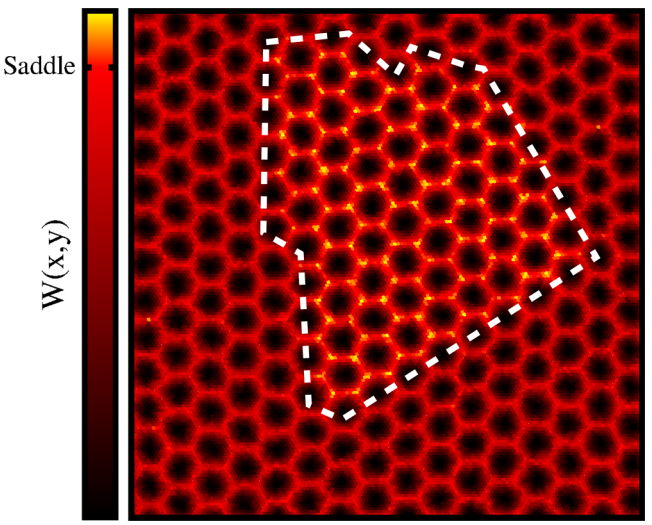

FIG. 8. Snapshot of a simulation performed at $T = 0.04$ and $W_1 < W_0 = 0.294 < W_2$, within the coexistence region. Each particle is colored according to the value of the underlying corrugation potential $W(x,y)$: dark for positions close to the minima, and light colors for positions close to the maxima of $W(x,y)$. The dashed line highlights a large portion of the simulation supercell where the colloidal lattice is in the unpinned phase. This can be seen by the presence of particles (bright yellow dots) residing in energetically unfavorable positions very close to the maxima of the substrate potential. The rest of the system is instead in the pinned phase, characterized by a nearly complete absence of particles residing close to the maxima.

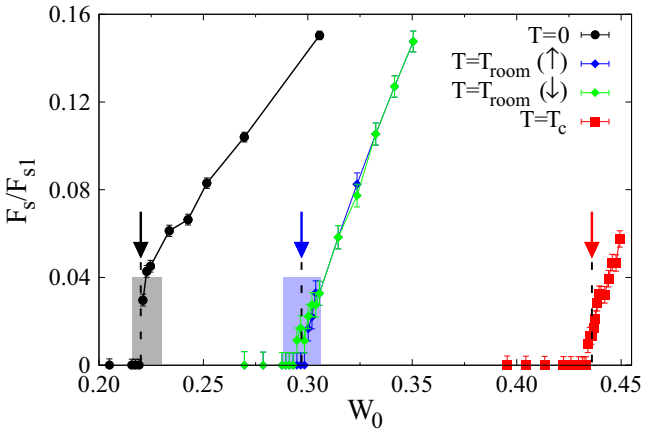

FIG. 9. The static friction force F_s, normalized with respect to the single-particle value $F_{s1} = 8\pi W_0/9a_l$ as a function of W_0 for three different temperatures $T = 0, 0.04\,(\sim T_{\rm room}), 0.11\,(\sim T_c)$. Shaded areas indicate the two-phase coexistence region extracted from the phase diagram of Fig. 4. The two curves at $T = T_{\rm room}$ are obtained upon increasing (decreasing) W_0, and are not meaningful inside the two-phase region, where the monolayer is inhomogeneous. The black, blue, and red arrows indicate the potential magnitudes $W_0^* \simeq 0.22$, 0.30, and $W_{0c} \simeq 0.44$, respectively, of the first-order transitions at $T = 0$ and $T = 0.04$, and of the $T = 0.11$ critical point. Note that the static friction jump, visible at $T = 0$, is still present at $T = 0.04$ (even if artificially smeared out by two-phase coexistence), while it disappears at $T_c \sim 0.11$, a temperature where static friction becomes continuous versus W_0. Error bars represent the ΔF step adopted in the protocol with increasing external homogeneous force F_d.

The result in Fig. 7 shows a sharp susceptibility peak at T_c, confirming the presence of a critical point. A finite-temperature critical Aubry transition is a major novelty predicted for this system. The nature of this critical point is quite interesting, and can be rationalized by analogy with the gas-liquid critical point. Just below the gas-liquid critical point, droplets of liquid coexist with large gas bubbles in the two-phase region. As the critical point is approached, the boundaries between gas and liquid get fuzzier and increasingly fluctuating, with length scales that eventually diverge. Here the situation is similar. Portions of the moiré honeycomb remain unpinned and even locally misaligned, others turn toward zero local angle and become pinned, as Fig. 8 shows. Eventually, their fluctuating and fuzzy boundaries of increasing width make the separation less and less clear until it disappears at the critical point.

What critical indices should this new critical point have? We try to anticipate the outcome by means of universality, which is based on symmetry. In a misaligned monolayer, the unpinned and the pinned states appear to share the same space group symmetry. In addition, once the global misalignment angle is fixed, thus taking care of all 60° rotations, there is no further symmetry left in either phase. This makes the analogy with gas liquid quite strong, suggesting that the unpinned-pinned critical point should be Ising-like. Present size and time limitations do not permit the extraction of critical indices from our simulations, and that task will remain for further work.

VI. STATIC FRICTION

The two monolayer phases below T_c are the finite-temperature continuations of the unpinned and pinned phases already studied at $T = 0$ [17]. As in that case, they are expected to exhibit, respectively, zero and finite static friction, defined as the minimal applied force that can cause sliding.

Figure 9 shows the static friction results at $T = 0$, 0.04 ($\sim T_{\rm room}$), and 0.11 ($\sim T_c$), obtained as explained in Sec. II. The lubricity of the small W_0 phase and the more frictional nature of the large W_0 phase are confirmed. However, the large static friction jump at $T = 0$ between the two phases is generally smeared with temperature, until at $T \sim T_c$ static friction appears already somewhat below the transition.

It can be expected that this overall behavior of the phases, probably with a sharp transition from viscous friction to stick slip should carry over to dynamic friction. This aspect will form the object of a future study.

VII. DISCUSSION AND CONCLUSIONS

The model study presented in this work establishes that a sharp unpinned-pinned transition for increasing periodic potential acting on an incommensurate lattice of particles, first established by Aubry in one dimension where it is of second order and strictly at $T = 0$, should carry over in two dimensions at $T > 0$. For the particular case of an incommensurate colloid system, which we model here, the transition can be even sharper, first order instead of second order, and extending to realistically finite temperatures. The transition is structural, with portions of the moiré turning from locally misaligned to aligned. The pinned phase correspondingly gains energy at the transition, while at the same time both interparticle energy and entropy suffer a corresponding loss, as shown by the large slope of the coexistence phase line. The phase line ends in a critical point, where the unpinned-pinned distinction disappears and fluctuations appear to diverge.

While obtained for a specific model and incommensurability, these results should qualitatively persist for more general parameter values. The magnitude of first-order jumps is connected with that of the Novaco angle, in turn related to the value of incommensurability ρ. By choosing $\rho < 0.927$, the first-order character, and with that the width of the two-phase coexistence region and the value of T_c, will increase. The frictional behavior changes from lubricity to pinning at the transition. The dynamical friction in the coexistence region constitutes an interesting question for further work.

The novel predicted critical point can and should be accessible experimentally. In fact, different incommensurabilities will imply different critical temperatures. Therefore, even if experimental temperature is by necessity fixed at its room value, a choice of ρ closer and closer to one can always be found, where $T_c \sim T_{\rm room}$, making the critical point fully accessible.

It will also be interesting in the future to study the nature and properties of the unpinned-pinned Aubry transition in, e.g., 2D systems different from colloid monolayers, such as could be realized by compressing two sheet materials together, or by modifying the adhesive interaction of 2D adsorbates layers by charging. The nature of these systems is sufficiently

different from colloid monolayers to suggest that there might be substantial differences, as well as analogies. In cases where the Novaco-McTague misalignment does not occur, all first-order characters of the transition might be weaker; but its existence at finite temperature should at least persist. We also expect that the precise nature of interparticle interactions will make a quantitative, but probably not a total difference. The 2D Aubry transition should persist, for example, in systems where interparticle interactions have an attractive part, so long as these do not lead to a 2D lattice collapse. The 2D Frenkel-Kontorova model in particular [9], still to be studied in this respect, should show an Aubry-type transition as well.

ACKNOWLEDGMENT

We are grateful to T. Brazda and C. Bechinger for much ongoing exchange of ideas and information, and to A. Silva and R. Guerra for discussion. This work was mainly supported under the ERC Advanced Grant No. 320796-MODPHYSFRICT, and by COST Action MP1303.

[1] A. Vanossi, N. Manini, M. Urbakh, S. Zapperi, and E. Tosatti, Rev. Mod. Phys. **85**, 529 (2013).
[2] N. Manini, O. M. Braun, E. Tosatti, R. Guerra, and A. Vanossi, J. Phys.: Condens. Matter **28**, 293001 (2016).
[3] M. Dienwiebel, G. S. Verhoeven, N. Pradeep, J. W. M. Frenken, J. A. Heimberg, and H. W. Zandbergen, Phys. Rev. Lett. **92**, 126101 (2004).
[4] I. Leven, D. Krepel, O. Shemesh, and O. Hod, J. Phys. Chem. Lett. **4**, 115 (2013).
[5] M. Pierno, L. Bruschi, G. Mistura, G. Paolicelli, A. di Bona, S. Valeri, R. Guerra, A. Vanossi, and E. Tosatti, Nature Nanotech. **10**, 714 (2015).
[6] T. Bohlein, J. Mikhael, and C. Bechinger, Nat. Mater. **11**, 126 (2012).
[7] A. Vanossi, N. Manini, and E. Tosatti, Proc. Natl. Acad. Sci. USA **109**, 16429 (2012).
[8] L. M. Floría and J. J. Mazo, Adv. Phys. **45**, 505 (1996).
[9] O. M. Braun and Y. Kivshar, *The Frenkel-Kontorova Model: Concepts, Methods, and Applications* (Springer, Berlin, 1998).
[10] S. Aubry and P. Y. Le Daeron, Physica D **8**, 381 (1983).
[11] S. N. Coppersmith and D. S. Fisher, Phys. Rev. B **28**, 2566 (1983).
[12] G. M. Mazzucchelli and R. Zeyher, Z. Phys. B **62**, 367 (1985).
[13] A. Benassi, A. Vanossi, and E. Tosatti, Nat. Commun. **2**, 236 (2011).
[14] D. Mandelli, A. Vanossi, and E. Tosatti, Phys. Rev. B **87**, 195418 (2013).
[15] D. Gangloff, A. Bylinskii, I. Counts, W. Jhe, and V. Vuletić, Nat. Phys. **11**, 915 (2015).
[16] A. Bylinskii, D. Gangloff, and V. Vuletić, Science **348**, 1115 (2015).
[17] D. Mandelli, A. Vanossi, M. Invernizzi, S. Paronuzzi, N. Manini, and E. Tosatti, Phys. Rev. B **92**, 134306 (2015).
[18] C. Reichhardt and C. J. O. Reichhardt, Rep. Prog. Phys. **80**, 026501 (2016).
[19] A. D. Novaco and J. P. Mc Tague, Phys. Rev. Lett. **38**, 1286 (1977).
[20] G. T. de Laissardière, D. Mayou, and L. Magaud, Nano Lett. **10**, 804 (2010).
[21] D. Mandelli, A. Vanossi, N. Manini, and E. Tosatti, Phys. Rev. Lett. **114**, 108302 (2015).
[22] F. Grey and J. Bohr, Europhys. Lett. **18**, 717 (1992).
[23] D. C. Johnston, *Advances in Thermodynamics of the van der Waals Fluid* (Morgan & Claypool Publishers, 2014).
[24] M. Henderson and M. S. Wertheim, J. Chem. Phys. **51**, 5420 (1969).